Journal of Great Lakes Research 45 (2019) 587–595

Contents lists available at ScienceDirect

Journal of Great Lakes Research

journal homepage: www.elsevier.com/locate/jglr

Extending the forecast model: Predicting Western Lake Erie harmful algal blooms at multiple spatial scales

Nathan F. Manning [a,*], Yu-Chen Wang [a], Colleen M. Long [a], Isabella Bertani [a], Michael J. Sayers [b], Karl R. Bosse [b], Robert A. Shuchman [b], Donald Scavia [c]

[a] University of Michigan Water Center, 214 S. State St., Ste. 200, Ann Arbor, MI 48104, USA
[b] Michigan Tech Research Institute, Michigan Technological University, 3600 Green Ct. Ste. 100, Ann Arbor, MI 48105, USA
[c] School for Environment and Sustainability, University of Michigan, 440 Church St., Ann Arbor, MI 48104, USA

ARTICLE INFO

Article history:
Received 9 July 2018
Accepted 14 March 2019
Available online 22 March 2019

Communicated by Joseph Ortiz

Keywords:
Lake Erie
Harmful algal blooms
Forecast modeling

ABSTRACT

Lake Erie is a classic case of development, recovery from, and return to eutrophication, hypoxia, and harmful algal blooms. Forecast models are used annually to predict bloom intensity for the whole Western Lake Erie Basin, but do not necessarily reflect nearshore conditions or regional variations, which are important for local stakeholders. In this study we: 1) developed relationships between observed whole basin and nearshore bloom sizes, and 2) updated and extended a Bayesian seasonal bloom forecast model to provide new regional predictions. The western basin was subdivided into 5 km near-shore regions, and bloom start date, size, and intensity were quantified with MODIS-derived images of chlorophyll concentrations for July–October 2002–2016 for each subdivision and for the entire basin. While bloom severity within each subdivision is temporally and spatially unique, it increased over the study period in each subdivision. The models for the 5 km subdivisions explained between 83 and 95% of variability between regional sizes and whole bloom size for US subdivisions and 51% for the Canadian subdivision. By linking predictive basin-wide models to regional regression estimates, we are now able to better predict potential bloom impacts at scales and in specific areas that are vital to the economic well-being of the region and allow for better management responses.

Introduction

Anthropogenic eutrophication of inland and coastal waterways is a global concern that has serious ecological and economic consequences (Hondorp et al., 2010, Breitburg et al., 2018). Many of the largest and most productive water bodies around the world are threatened with habitat loss and decreasing biodiversity, leading to public health risks and reductions in economic output (Brooks et al., 2017). In many cases, nutrient over-enrichment has created systems favorable for producing low oxygen (hypoxic) bottom waters in vertically stratified systems and proliferation of several species of colonial cyanobacteria (Heisler et al., 2008). Often referred to as harmful algal blooms (HABs), these cyanobacteria colonies impact virtually every aspect of a system's ecological and economic value, from degrading aquatic habitat through light limitation to impairing recreational use due to surface scum formations. In some cases colonies produce toxins that endanger the health of organisms that live in the system as well as people that depend on the water body for food and drinking water (Otten and Paerl, 2015).

Lake Erie is a classic case of development, recovery from, and return to eutrophication, hypoxia, and HABs. Substantial increases in nutrient loading from agricultural, industrial, and urban sources in the mid-20th century led to severe water quality degradation in the 1960's (Rosa and Burns, 1987; Bertram, 1993; Makarewicz et al., 1989). These highly publicized problems ultimately led the governments of the United States and Canada to shape a Great Lakes Water Quality Agreement (GLWQA, 1978) with a focus on phosphorus (P) load reduction. The subsequent P abatement programs led to a relatively quick recovery (DePinto et al., 1986) as indicated by decreases in total phosphorus (TP) loads (Dolan, 1993), water column TP concentrations (DePinto et al., 1986; Ludsin et al., 2001), phytoplankton biomass (especially western basin cyanobacteria), and central basin bottom-water hypoxia (Makarewicz and Bertram, 1991; Bertram, 1993; Charlton et al., 1993), as well as by recovery of several ecologically and economically important fishes (Ludsin et al., 2001).

These improvements were relatively short lived, however, because hypoxia and HAB biomass began to increase during the 1990's (Scavia et al., 2014). There has been a return of extensive central basin hypoxia (Burns et al., 2005; Zhou et al., 2013; Rucinski et al., 2014) and increases

* Corresponding author at: National Center for Water Quality Research, Heidelberg University, 310 E. Market St., Tiffin, OH 44883, USA.
E-mail address: manningn@umich.edu (N.F. Manning).

https://doi.org/10.1016/j.jglr.2019.03.004
0380-1330/

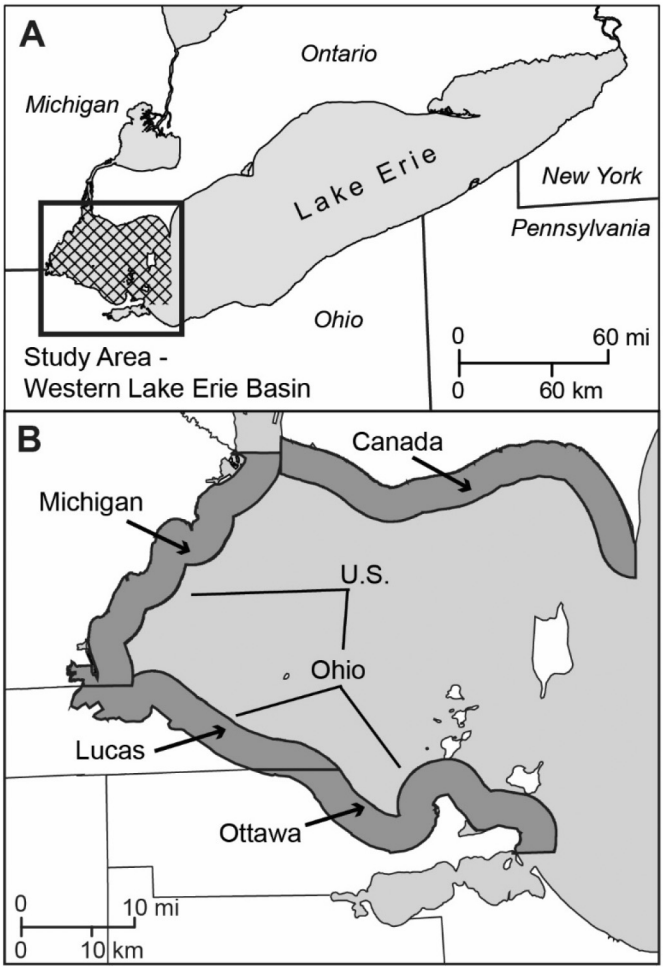

Fig. 1. Map of (A) Lake Erie and (B) the western basin, with the 5 km nearshore regions defined for this study. Hatched area denotes the extent of western basin used for this study.

in cyanobacteria blooms in the western basin (e.g. *Microcystis* spp. and *Lyngbya wollei*) (Bridgeman et al., 2012; Stumpf et al., 2012; Michalak et al., 2013), with record blooms set in 2011 (Michalak et al., 2013) and 2015, and a bloom in 2014 that led to a "do not drink" advisory for 400,000 people living in the Toledo, OH area.

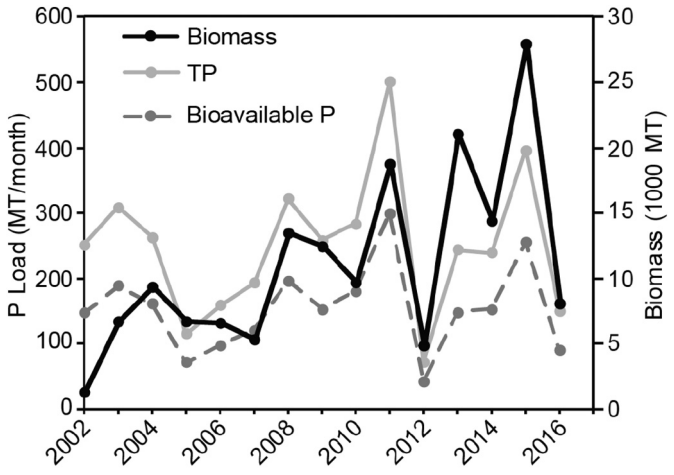

Fig. 2. MODIS derived bloom biomass estimates and spring total phosphorus and bioavailable phosphorus loads to the western basin of Lake Erie 2002–2016. Loading data acquired from the National Center for Water Quality at Heidelberg University, Tiffin, Ohio, USA.

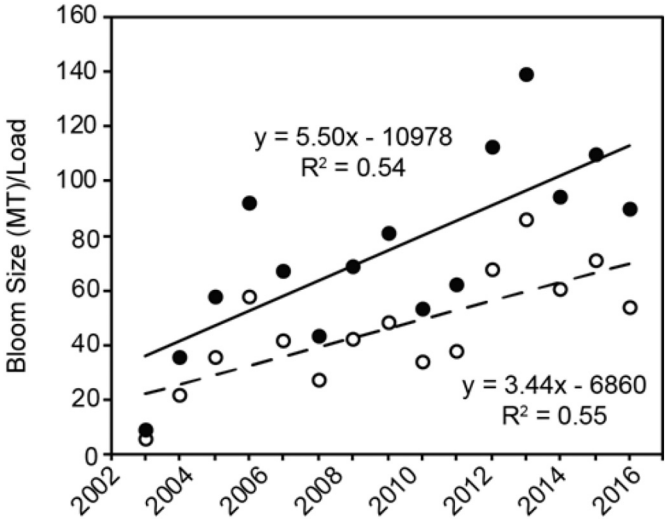

Fig. 3. Bloom sensitivity (bloom size/load) for total phosphorus (open circles) and bioavailable phosphorus (filled circles) for the years 2002–2016. The P value for both lines was $P < 0.001$.

This degradation in water quality prompted the US and Canada to revise the GLWQA and set new P load reduction targets (GLWQA, 2016), and they are developing domestic action plans (IJC, 2017) to reach those targets over the long term. Shorter-term actions include producing seasonal HAB forecasts that predict the severity of the late summer maximum bloom biomass as a function of spring P loads from the Maumee River watershed, the primary HAB driver (Obenour et al., 2014; Bertani et al., 2016; Stumpf et al., 2016; Verhamme et al., 2016). While these forecasts help the water supply, fishing, and recreation communities prepare for severe blooms, to date the forecasts only estimate the severity of the overall bloom, not its expected location. To address this shortcoming, we present an approach that extends the existing HAB forecast models in Western Lake Erie by relating their predictions of basin-wide bloom sizes to the corresponding bloom sizes in nearshore regions derived from MODIS imagery. This results in predictions at smaller spatial scales that are more useful to management entities, stakeholders, and the general public.

Despite an unremarkable bathymetry, Lake Erie's western basin has significant spatial heterogeneity driven by winds, hydrodynamics, and the distribution of tributary loads that plays a key role in bloom

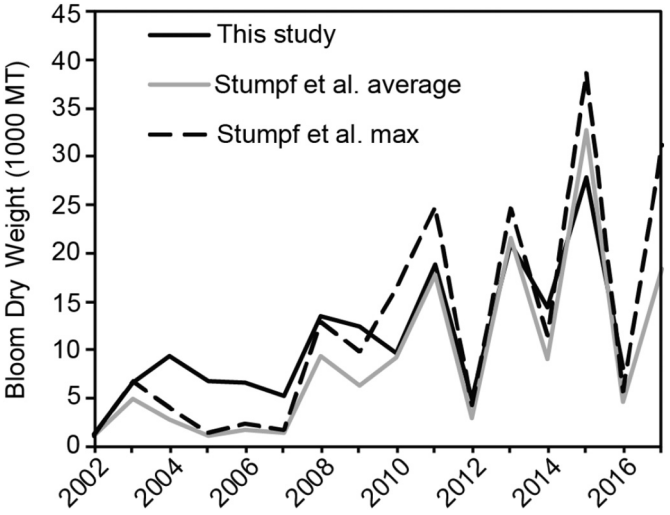

Fig. 4. MODIS derived bloom size estimates from the Michigan Tech Research Institute (MTRI) data used in this study compared to estimates used in previous studies (Stumpf et al., 2016).

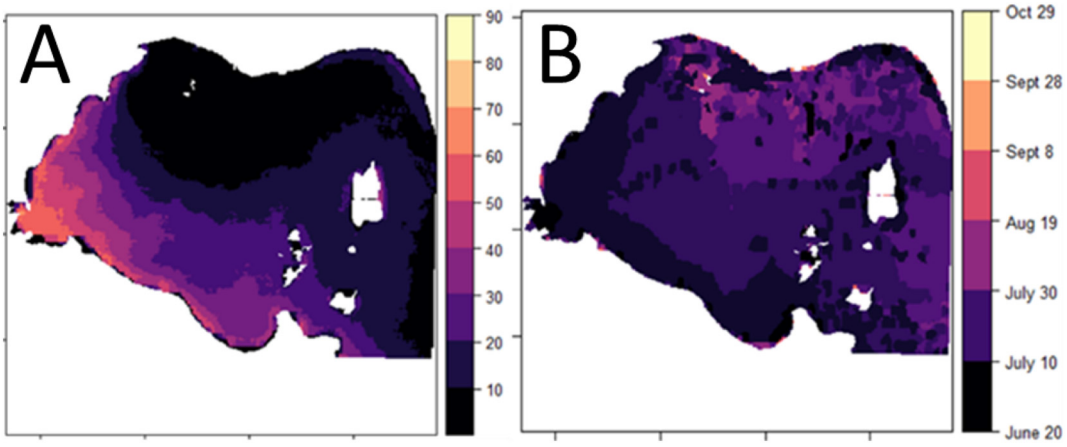

Fig. 5. Spatial distribution of HAB characteristics for 2002–2016. (A) The percentage of images with a HAB presence July–October. (B) Date of earliest HAB occurrence across study period. For each map, presence of HAB is defined as chlorophyll concentration > 18 μg/l.

development and distribution (Jiang et al., 2015). For example, the two major tributaries entering the western basin, the Maumee and Detroit Rivers, differ widely in flow, total suspended solids, and P concentrations (Reichert et al., 2010). The contrast between these tributaries produces a southern shore dominated by the warm, turbid water of the Maumee, and a northern shore reflecting the colder, clearer water of the Detroit River (Reichert et al., 2010). In the early years of the resurgent western basin HABs, this difference in composition and flow of the Detroit and Maumee water masses kept blooms typically along the southern shore. In more recent years, however, blooms have been recorded in the Detroit River plume and along the northern shore. Thus, the potential ecological, economic, and public health impacts are now no longer focused only on the southern shore. Because of this shift in the scale and location of potential impacts, it is important to understand and predict bloom size and intensity not only at the basin scale, but also in different regions within the basin.

The primary goals of this study were: 1) To use daily MODIS images that estimate chlorophyll concentration across the western basin to develop regression models that predict local bloom size in nearshore regions as a function of basin-wide bloom size, and 2) To showcase the application of these regional regression models by linking them to an updated version of an existing Bayesian basin-wide bloom forecast model.

Materials and methods

Study area

The western basin of Lake Erie (Fig. 1) is a large (~6500 km^2), shallow (average depth ~7 m), highly productive system that provides a wide range of valuable ecosystem services as an important part of the economies of Ohio, Michigan, and southern Ontario (Allan et al., 2017). Between the two major tributaries, the Detroit River's average discharge (5324 m^3/s) is much higher than the Maumee's (150 m^3/s), but they deliver comparable P loads (41 and 48% of the total annual load to the western basin, respectively). However, the higher P concentration in the Maumee River (Ohio EPA, 2010) makes it a much stronger driver of bloom development (Scavia et al., 2014; Obenour et al., 2014; Bertani et al., 2016; Stumpf et al., 2016; Verhamme et al., 2016). In addition, a number of smaller tributaries and a series of islands along the eastern edge of the basin contribute to significant spatial and seasonal variability in water quality and conditions.

For our regional analyses, we divided the western basin into six 5 km near-shore bands following existing political boundaries (Fig. 1). We use 5 km bands, as opposed to other methods of delineating nearshore from offshore, because most biological resources (Vadeboncoeur et al., 2011) and human activities are concentrated along the shoreline, and nearshore influence on water quality attenuates at ~3–5 km (Kelly

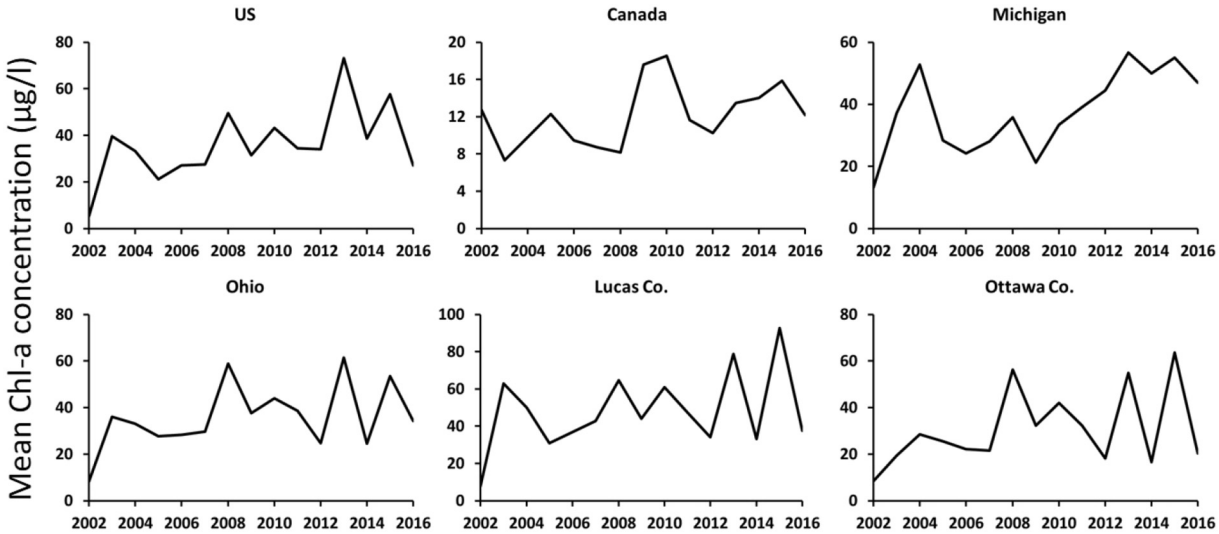

Fig. 6. Trends in the mean MODIS derived chl-a concentrations (μg/l) for each region for the years 2002–2016.

Table 1
Regional mean chl-a concentrations (μg/l), with minimum (light shades) and maximum (dark shade) for each region and the whole western basin.

	Canada 5km	US 5km	MI 5km	OH 5km	Lucas 5km	Ottawa 5km	Whole basin
2002	12.72	5.35	13.21	8.22	7.92	8.45	4.78
2003	7.32	39.72	37.09	36.03	62.95	19.38	20.21
2004	9.80	33.25	52.78	33.04	50.00	28.60	15.25
2005	12.30	21.26	28.32	27.77	30.83	25.57	9.92
2006	9.46	27.03	24.15	28.35	36.90	22.20	15.02
2007	8.74	27.54	28.09	29.78	42.94	21.47	11.81
2008	8.19	49.57	35.83	58.88	64.73	56.32	22.09
2009	17.62	31.48	21.22	37.62	44.00	32.29	19.57
2010	18.55	43.28	33.38	44.02	60.96	41.95	19.65
2011	11.65	34.56	39.09	38.58	47.37	32.26	26.07
2012	10.25	34.02	44.52	24.73	34.05	18.15	11.17
2013	13.48	73.09	56.64	61.56	78.73	54.99	30.46
2014	14.03	38.62	49.96	24.46	33.20	16.58	21.40
2015	15.86	57.70	55.06	53.51	92.78	63.61	36.70
2016	12.20	27.09	46.97	34.32	37.65	20.45	13.56

et al., 2015). Furthermore, land-based biological resources are dependent on lake conditions to a distance of ~2–5 km (Pearsall et al., 2012; Bonter et al., 2009). The lowest resolution bands are along the Canadian and US shores. The next highest resolution divides the US shoreline along the Michigan and Ohio border, and the final resolution divides the Ohio shoreline into Lucas and Ottawa County bands.

HAB bloom estimates

Bloom start date, extent, and intensity for the entire western basin and for the individual regions were quantified with MODIS-derived images of chlorophyll concentrations for July–October 2002–2016 developed by Sayers et al. (2016). For our analyses, we cropped images to

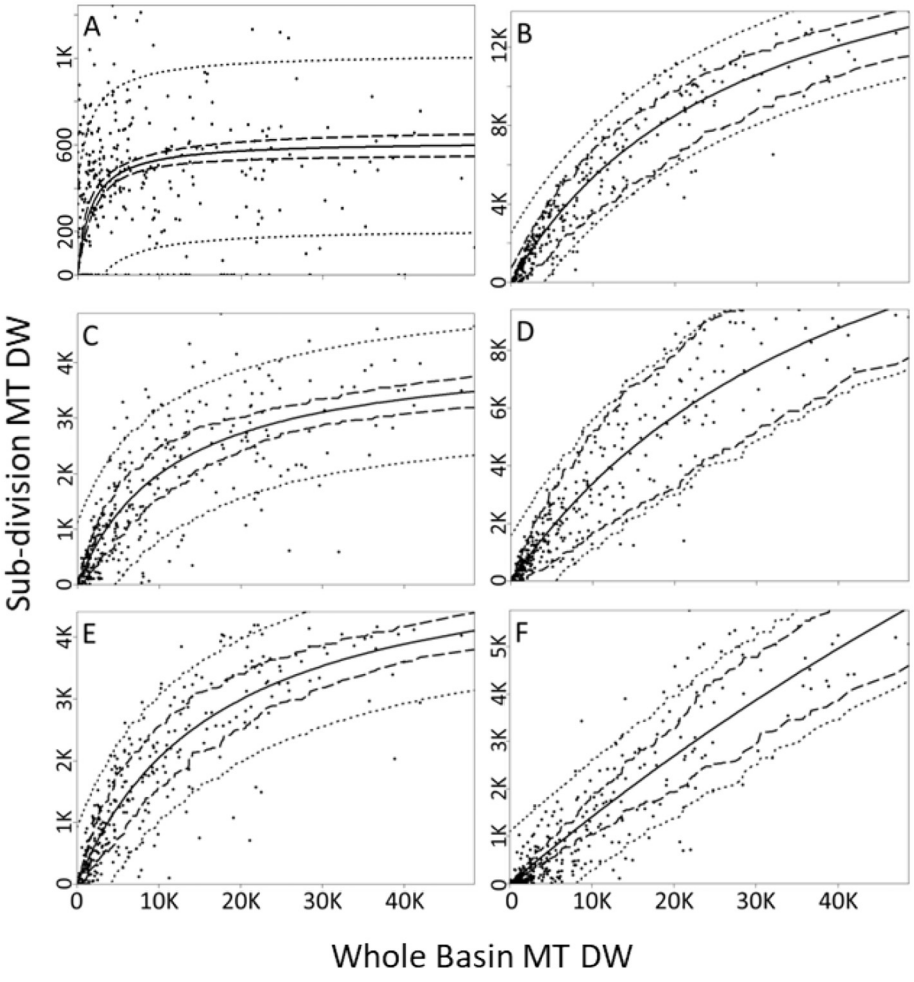

Fig. 7. Regression curves for the 5 km buffers for Canada (A), US (B), Michigan (C), Ohio (D), Lucas County (E), and Ottawa County (F). Solid line is the prediction, dotted lines represent the 90% prediction intervals, and dashed lines represent the 90% confidence intervals.

Table 2
Regional regression results for the Monod models. The Monod equation is $\mu = \mu_{max}\frac{S}{KS+S}$ where μ_{max} is the maximum regional bloom extent (μ, MT) achieved by the system at saturation, K is the half-saturation constant, and S is the whole-basin bloom extent (MT).

	Model coefficients	
Subdivision	K	Max
Canada 5 km	6.181	1635.988
US 5 km	20,714.000	28,713.000
Michigan 5 km	4320.400	11,681.799
Ohio 5 km	18,661.000	45,161.000
Lucas Co. 5 km	5568.100	17,258.000
Ottawa Co. 5 km	31,286.000	212,431.000

the western basin (defined as the region west of a line connecting Point Pelee, Ontario with Marblehead, Ohio), and re-projected the original latitude/longitude coordinate system into UTM-Zone 17N. In some instances, data were only available at the 1000-m pixel scale, and so to match the resolution of the other MODIS products, these were rescaled to 250-m using bilinear interpolation. To assess the potential influence of spatial rescaling on bloom estimates, we calculated the mean and standard deviation of the chlorophyll values from all pixels in each image both before and after resampling, and conducted a regression analysis for the average and standard deviation using values after the resampling as the predictor. The R-squared and slope coefficient were close to 1, suggesting the resampling did not affect overall chlorophyll concentration estimates. The minimum value for each pixel was set to the minimum background chlorophyll concentration found in the Great Lakes during the growing season (0.15 μgChl/l; Fahnenstiel et al., 2016). Because the land-lake boundary was not the same in each image, we created and applied a mask of the western basin to all images to make the area of analysis consistent.

The pixel values of each image were subset for each subdivision described above. Because cloud cover could affect one region and not another, if a subdivision had <20% observable area, the data from that day would be dropped for that region, but retained for other regions. Additionally, a fixed model pair aerosol correction and custom cloud masking approach was used to limit the influence of atmospheric contamination on reflectance values in the selected images (Sayers et al., 2016). For both regional regression analyses and whole-basin maximum bloom estimates, we only used images from July–October because HABs usually occur after July (Wynne and Stumpf, 2015).

When chlorophyll concentration is above 18 μg/l and water temperature is >20 °C, the phytoplankton is overwhelmingly dominated by cyanobacteria (Sayers et al., 2016), and we therefore used these two thresholds to ensure that we were identifying cyanobacteria and no other phytoplankton in our analyses. To estimate total mass of cyanobacteria chlorophyll for each region, we summed chlorophyll concentrations for all pixels whose values were above 18 μg/l and multiplied the sum by the pixel area (0.0625 km^2) and a sensor optical depth of 1 m (Wynne et al., 2010; Stumpf et al., 2016). Chlorophyll mass was then converted to dry weight with a *Microcystis* chlorophyll to dry weight ratio of 0.0038 (Lee et al., 2000, Long et al., 2001, Chaffin, 2009, Chong et al., 2010, Chen et al., 2011). Annual estimates of peak HAB dry weight were determined as the maximum of 21-day rolling averages after linear interpolation of observations to fill in days with no MODIS data and setting bloom areas to zero for temperatures below 20 °C at the start of the bloom and below 16 °C for bloom termination. These temperatures represent thresholds at which cyanobacteria begin to dominate the planktonic community, and are no longer competitively dominant, respectively (Bridgeman et al., 2012; Sayers et al., 2016). Daily western basin water temperatures were estimated by adjusting lake-wide averages (http://tinyurl.com/ycv6uzh5) with polynomial regressions based on western basin observations made during summer sampling (http://tinyurl.com/y9nn9amn).

We compared our annual basin-wide HAB estimates to those obtained by Stumpf et al. (2016). In that study, HAB size is expressed in terms of a Cyanobacteria Index (CI), which we converted to dry weight metric tons (MT) to match the output of our predictive model by multiplying by 2000 based on the definition of CI as 10^{20} cells and the dry weight of *Microcystis* cells (20 pg/cell; Long et al., 2001, Dunker et al., 2013, Hu, 2014). Because we want these regional estimates to act as extensions of the current annual bloom forecast (http://tinyurl.com/yadcqyeb), we then converted our dry weight values to an index that mirrors the 1–10 scale used in the bloom forecast. Our Regional Biomass Index (RBI) is scaled to minimum and maximum bloom sizes for each region during the study period as:

$$RBI = [((MT)-(MT_{min}))/((MT_{max}-(MT_{min}))] \quad (1)$$

Statistical analyses

Relationships between regional bloom biomass and that of the whole basin were developed using the *nls* function in R (R Core Team, 2016). For these analyses, all of the chlorophyll images which fit the criteria described above were used. The Canadian data exhibited a strong positive skew, and thus were transformed using the Tukey's

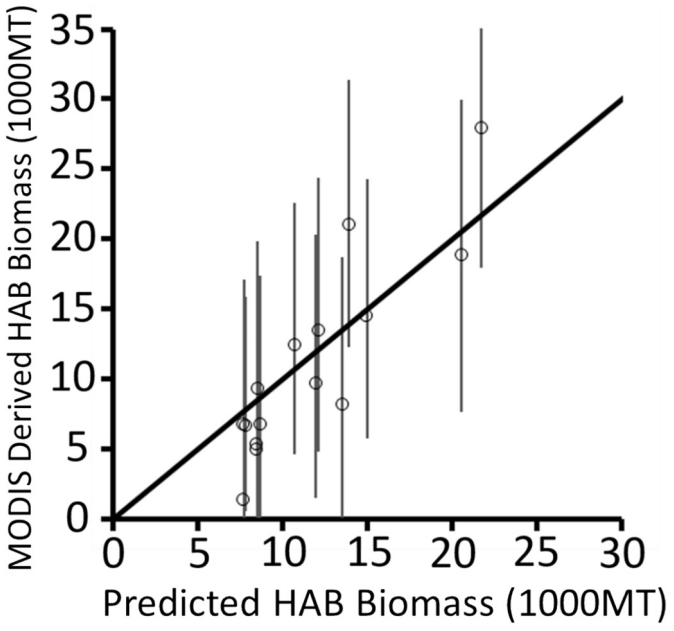

Fig. 8. Model estimates vs. MODIS derived whole–basin HAB biomass. The open circles are the intersection between model predictions and observed values. The dark line represents the 1:1 relationship and the thin vertical lines represent the 90% predictive interval for each prediction. In these plots, the 90% predictive intervals account for measurement uncertainty, prediction uncertainty, and model parameter uncertainty, such that they represent the likely range of bloom observations corresponding to each model prediction.

Table 3
Posterior parameter means and 95% Credible Intervals for the Bayesian model.

Parameter	Units of measurement	Mean	95% CI
β_0	1000 MT	−11.15	−45.99–6.37
β_w	1000 MT/(1000 MT/month)	71.36	15.1–165.41
β_b	1000 MT	6.85	0.82–11.34
β_t	1000 MT/year	1.28	0.10–3.75
β_ψ		3.08	1.08–5.74
σ_γ	1000 MT	5.04	3.17–7.53
θ		0.51	0.21–0.95

ladder of powers transformation (*transformTukey* function in R), which selects a lambda value that maximizes the Shapiro-Wilks W statistic. The lambda selected for the 5 km Canadian subdivisions was 0.325, similar to the value of a cube root transformation. A suite of regression models was developed for each subdivision, including Monod, power, exponential, and linear models. The best fit model for each subdivision was selected based on the Bayesian Information Criterion (BIC). As with all models, these regressions are limited by the available data, and as the data sets grow in the future, the type of model selected could change. Additionally, using BIC to select between different model types can present issues when the number of observations is low because it has a tendency to favor excessively simple models (Weakliem, 1999). The 90% confidence and prediction intervals for each best fit model were generated using the *predict* function for linear models and *predictNLS* function for nonlinear models in R. While 95% confidence intervals are typically used for scientific statistical assessment, we believe 90% is more consistent with the information typically used by our intended management and policy users. Therefore, we use 90% confidence and prediction intervals throughout.

Bayesian HAB model

To demonstrate how the output of an existing whole-basin forecasting model can be used to make regional bloom predictions, we used the probabilistic forecasting model developed by Obenour et al. (2014) and revised by Bertani et al. (2016). This model predicts peak late-summer bloom size in Western Lake Erie based on spring (March–June) nutrient load from the Maumee River and a temporal trend that reflects the lake's apparent increasing susceptibility to HABs. The model is solved within a Bayesian hierarchical framework that allows for simultaneous calibration to multiple sets of bloom observations and for a differentiation between model prediction (i.e., process) error and bloom measurement error (Obenour et al., 2014). For our study, however, we use the single set of MODIS-derived observations.

The deterministic component of the model is as follows:

$$\hat{z}_i = \begin{cases} \beta_b + \beta_0 + \beta_w W_i + \beta_t T_i & \text{for } \beta_0 + \beta_w W_i + \beta_t T_i > 0 \\ \beta_b & \text{for } \beta_0 + \beta_w W_i + \beta_t T_i < 0 \end{cases} \quad (2)$$

where β_b, β_0, β_w, and β_t are model parameters that predict bloom size, $\hat{z}_i$, in year i, in terms of spring nutrient load, W_i, and model year, T_i. The parameter β_b is a background bloom level representing bloom size in years with a small nutrient load. As load increases beyond a critical threshold, the size of the bloom increases as a linear function of the load, and the parameter β_w represents the unit increase in bloom size per unit increase in load. The parameter β_0 is an intercept term, and $\beta_t T_i$ essentially allows the intercept to change over time. The lake's increasing susceptibility to HABs is reflected by a positive value of β_t such that the intercept increases gradually over time (Obenour et al., 2014). The intercept is inversely related to the load threshold required to increase bloom size beyond the background level.

The original model was revised to accommodate the single set of MODIS bloom observations z_i, which are modeled as a gamma distribution:

$$z_i \sim Gamma\left[\hat{z}_i{}^2/\sigma_\gamma^2, \hat{z}_i/\sigma_\gamma^2\right] \quad (3)$$

where σ_γ^2 represents residual model error.

For each year i, the spring nutrient load is determined as a weighted average of January to June ($m = 1$ to 6) monthly loads $w_{i,m}$, based on the following equations:

$$W_i = \frac{1}{\sum \psi_m} \sum_{m=1}^{6} w_{i,m} \psi_m \quad (4)$$

$$\psi_m = \begin{cases} 0 & \text{for } m \le \left(\beta_\psi - 1\right) \\ m + 1 - \beta_\psi & \text{for } \left(\beta_\psi - 1\right) < m < \beta_\psi \\ 1 & \text{for } m \ge \beta_\psi \end{cases} \quad (5)$$

where β_ψ is a weighting parameter estimated probabilistically within the model. A more detailed description of the model formulation can be found in Obenour et al. (2014).

Bioavailable phosphorus load

The model was calibrated using the spring Maumee River bioavailable P load (Bertani et al., 2016), defined as the sum of the bioavailable portions of the dissolved reactive P (DRP) and particulate P (PP) loads (Lee et al., 1980; Baker et al., 2014):

$$W_i = Bioavailable\ P_i = \eta DRP_i + \theta PP_i \quad (6)$$

TP and DRP loads for the period 2002–2016 were estimated from Maumee River nutrient concentration data measured by Heidelberg University's National Center for Water Quality Research (NCWQR, http://www.heidelberg.edu/academiclife/distinctive/ncwqr/data, accessed on 31 May 2017), and stream flow data measured by the United States Geological Survey (USGS, http://www.usgs.gov/water, accessed on 31 May 2017) using the same methods outlined in Obenour et al. (2014). The PP load was approximated as the difference between the TP and DRP loads (Baker et al., 2014). Because DRP is expected to be approximately 100% readily available to algae, we set $\eta = 1$ (Lambert, 2012). Only a fraction (θ) of the PP load is expected to become available to algae. The parameter θ was thus estimated probabilistically, together with other model parameters, through Bayesian inference.

Model cross validation

To assess the model's performance when predicting conditions not included in the calibration process, we performed a leave-one-year-out cross validation, wherein observations from one year were removed from the dataset one at a time in turn, and the re-calibrated model was used to predict the excluded observations (Obenour et al., 2014).

Table 4
Regional Forecasts Dry Weight Biomass (MT), Regional Biomass Index (RBI), and 90% CI for a nominal whole-basin bloom extent of 25,000 MT. Negative values correspond to RBI below current minimum for that region.

Subdivision	Dry weight	90% CI	RBI	90% CI
Canada 5 km	447	375–500	0.05	0.02–0.08
US 5 km	9641	7500–11,000	0.4	0.2–0.6
Michigan 5 km	2950	2650–3200	0.3	0.2–0.4
Ohio 5 km	6649	4500–9000	0.4	−0.03–0.9
Lucas Co. 5 km	3294	300–3700	0.5	−0.9–0.7
Ottawa Co. 5 km	3294	2500–4200	0.3	0.04–0.5

Results and discussion

Annual peak bloom and load estimates

Estimates from the MODIS-derived data show that maximum bloom sizes were relatively small in the early years of the study period and increased significantly thereafter, with particularly large blooms in 2011, 2013, and 2015, corresponding with the inter-annual variability in TP (R^2=0.401, P = 0.011) and bioavailable P load (R^2 = 0.439, P = 0.007) (Fig. 2). The ratio of bloom size to the P load (Fig. 3, Electronic Supplementary Material (ESM) Fig. S1) confirms the increased load sensitivity of blooms first identified by Obenour et al. (2014). That is, the unit increase in bloom size per unit increase in load increased over time. While our approach for estimating peak blooms size differs considerably from Stumpf et al. (2016), our estimates are similar to theirs based on both their maximum 10-day composite bloom size (R^2 = 0.898, P < 0.001) and their 30-day average of 10-day composites (R^2 = 0.915, P < 0.001) (Fig. 4). In addition to defining the peak bloom differently, Stumpf's algorithm isolates cyanobacteria, whereas ours is based on chlorophyll concentrations above 18 μg/l. As such, our relatively higher estimates at lower blooms sizes (e.g., 2004–2007) may reflect the presence of non-cyanobacteria at low chlorophyll concentrations.

Regional dynamics

The spatial distributions of HAB frequency and start dates illustrate the importance of understanding and predicting blooms in specific subdivisions (Fig. 5). Each subdivision has distinct dynamics and trends (Fig. 6, Table 1, ESM Table S1). While chlorophyll concentrations within each subdivision are both temporally and spatially unique, each subdivision showed increasing severity over time. For example, in five of the six subdivisions the lowest concentrations were recorded in 2002, and the Canadian subdivision had its lowest concentration in 2003. In contrast, five of the six subdivisions had their highest concentrations in 2013 or later, and none had their maximum prior to 2010. Additionally, concentrations after 2008 are, on average, 73.7% higher than the pre-2008 values, with a minimum of +68.5% in the US subdivision, and a high of +79.6% in the Ohio subdivision.

Regional regression results

Based on pairs of estimates of regional and basin-wide bloom biomass, a nonlinear, saturating function (Monod) was selected as the best model for all subdivisions (Fig. 7, Table 2). The models explained between 83% and 95% of the variability for the US subdivisions and 51% for the Canadian subdivision. This suggests that given the annual whole-basin bloom forecast, we can now make strong predictions of bloom size at new, smaller regional scales, particularly for nearshore areas on the US side of the lake, which is much more affected by the nutrient-rich Maumee River plume. The Canadian results reflect the more complex environmental conditions that influence north-shore blooms. While whole-basin bloom size does explain a majority of the variance seen in the data, other factors not included in this analysis, like the influence of the Detroit River plume, or direction and intensity of the prevailing winds, can influence the size of the bloom observed in the Canadian nearshore region.

Basin-wide forecasts

The Bayesian forecasting model driven with bioavailable P performed well with this single data set calibrated through 2016 (R^2 = 72.2%, P < 0.001, Fig. 8), although it explained less of the inter-annual variability than the original TP and DRP models that were calibrated to multiple data sets through 2013 (TP model: R^2 = 91.9%; DRP model: R^2 = 88.0%) (Obenour et al., 2014) and the updated bioavailable P model calibrated through 2014 (R^2 = 84.2) (Bertani et al., 2016). Model skill when performing a leave-one-year-out cross validation (CV-R^2 = 62.4%, P < 0.001) decreased relative to the Obenour et al. and Bertani et al. models (CV-R^2 = 83.8% and CV-R^2 of 69.8%, respectively), but is still acceptable. Posterior parameter mean estimates (Table 3) were within the credible intervals from Bertani's bioavailable P model, with the exception of the temporal trend parameter (β_t), which is still positive and significant but lower than Bertani et al. (2016).

As part of developing load reduction targets, cyanobacteria blooms in Western Lake Erie were classified as "severe" when they reached an overall biomass >9600 MT (Scavia et al., 2014), which corresponds to a TP load of 860 MT for March–July, or 215 MT/month. This model predicts that under 2008 lake conditions, a spring Maumee TP load below 230 MT/month would be necessary to keep peak summer bloom size smaller than 9600 MT, which is consistent with results reported in Bertani et al. (2016) and similar to the current target. However, because of increased sensitivity to loading, the model run with the 2016 temporal term would result in a bloom substantially larger than 9600 MT with the same 230 MT/month load. Furthermore, under 2016 conditions, a load reduction of 40% from the 2008 baseline (i.e., the GLWQA target) would still result in blooms that are far larger the goal of blooms no >2004 or 2012 levels 90% of the time.

Regional forecasts

To demonstrate the utility of bloom forecasts for individual regions, we use a nominal basin-wide forecast of 25,000 MT, corresponding to a TP load of 690 MT/month. For a bloom this size, we would expect RBI values of 0.3 in the Michigan and Ottawa County subdivisions and 0.5 in the Lucas County subdivision (Table 4), but only 0.05 in the Canadian subdivision (Table 4). This demonstrates the need for regional forecasting, as the whole-basin estimate can result in drastically different relative impacts, even in neighboring regions like Lucas and Ottawa counties.

While reports of HABs to the Ontario Ministry of the Environment and Climate Change have increased since 1994 (Winter et al., 2011), in many instances the blooms observed near the northern shore were the result of extremely large blooms that extend from the mouth of the Maumee to the Canadian shore and the central basin. Unlike the bloom size relationships for the US regions, which saturate and reflect blooms covering the entirety of the subdivision even at relatively low basin-wide bloom sizes, the rate of saturation for the Canadian relationships is much slower, with large basin-wide blooms generally required to have a significant impact on the Canadian shoreline. The difference in bloom impacts on the US and Canadian regions are largely due to the effects of prevailing winds and the cold, relatively nutrient-poor Detroit River plume. However, any protection that the Detroit River plume may have provided to the northern shore in the past through reduced nutrient concentrations and cooler water temperatures may not be enough to prevent blooms on the northern shore in the future, as demonstrated by the 69% increase in average chl-a concentrations for the Canadian subdivision since 2008. Eutrophication, changes in food web dynamics due to invasive species, and climate change may all contribute to increasing HAB susceptibility along the northern shore (Pick, 2016).

Using output from the existing basin-wide bloom forecasts to develop regional forecasts provides managers and the public with more focused (and more useful) bloom estimates in areas of high use and value. Relatively small basin-wide blooms can still be significant in specific nearshore areas, and as such low whole-basin bloom severity estimates may provide a false sense of security to managers and the public. The western basin of Lake Erie is a dynamic system with significant economic and ecological importance and is under threat from a wide range of factors, not least of which are the impacts of harmful algal blooms. By linking existing predictive basin-wide models to regional regression estimates of bloom impact, we are now able to predict impacts of a bloom

at scales and in regions that are vital to the economic well-being of the region and allow for better management responses.

Acknowledgements

This project was funded by the National Science Foundation Coastal SEES grant (#OCE-1600012), the University of Michigan Water Center grants (#3003032930 and #3004701270), and the University of Michigan's Graham Sustainability Institute. We would like to thank Dan Obenour for his critical reviews of earlier drafts, and Richard Stumpf and Tom Bridgeman for access to their data.

Author contributions

The manuscript was written through contributions of all authors. All authors have given approval to the final version of the manuscript.

Funding sources

This work was supported by the National Science Foundation Coastal SEES grant (#OCE-1600012), the University of Michigan Water Center grants (#3003032930 and#3004701270).

Appendix A. Supplementary data

Supplementary data to this article can be found online at https://doi.org/10.1016/j.jglr.2019.03.004.

References

Allan, J.D., Manning, N.F., Smith, S.D., Dickinson, C.E., Joseph, C.A., Pearsall, D.R., 2017. Ecosystem services of Lake Erie: spatial distribution and concordance of multiple services. J. Great Lakes Res. 43 (4), 678–688.

Baker, D.B., Confesor, R.B., Ewing, D.E., Johnson, L.T., Kramer, J.W., Merryfield, B.J., 2014. Phosphorus loading to Lake Erie from the Maumee, Sandusky and Cuyahoga rivers: the importance of bioavailability. J. Great Lakes Res. 40, 502–517.

Bertani, I., Obenour, D.R., Steger, C.E., Stow, C.A., Gronewold, A.D., Scavia, D., 2016. Probabilistically assessing the role of nutrient loading in harmful algal bloom formation in western Lake Erie. J. Great Lakes Res. 42 (6), 1184–1192.

Bertram, P.E., 1993. Total phosphorus and dissolved oxygen trends in the central basin of Lake Erie, 1970–1991. J. Great Lakes Res. 19, 224–236.

Bonter, D.N., Gauthreaux Jr., S.A., Donovan, T.M., 2009. Characteristics of important stopover locations for migrating birds: remote sensing with radar in the Great Lakes basin. Conserv. Biol. 23 (2), 440–448.

Breitburg, D., Levin, L.A., Oschlies, A., Grégoire, M., Chavez, F.P., Conley, D.J., Garçon, V., Gilbert, D., Gutiérrez, D., Isensee, K., Jacinto, G.S., 2018. Declining oxygen in the global ocean and coastal waters. Science 359 (6371) (p.eaam7240).

Bridgeman, T.B., Chaffin, J.D., Kane, D.D., Conroy, J.D., Panek, S.E., Armenio, P.M., 2012. From River to Lake: phosphorus partitioning and algal community compositional changes in Western Lake Erie. J. Great Lakes Res. 38 (1), 90–97.

Brooks, B.W., Lazorchak, J.M., Howard, M.D., Johnson, M.V.V., Morton, S.L., Perkins, D.A., Reavie, E.D., Scott, G.I., Smith, S.A., Steevens, J.A., 2017. In some places, in some cases, and at some times, harmful algal blooms are the greatest threat to inland water quality. Environ. Toxicol. Chem. 36 (5), 1125–1127.

Burns, N.M., Rockwell, D.C., Bertram, P.E., Dolan, D.M., Ciborowski, J.J.H., 2005. Trends in temperature, secchi depth, and dissolved oxygen depletion rates in the central basin of Lake Erie, 1983–2002. J. Great Lakes Res. 31 (Supplement 2), 35–49.

Chaffin, J.D., 2009. Physiological ecology of Microcystis blooms in trubing waters of western Lake Erie. PhD Thesis. University of Toledo, Ohio.

Charlton, M.N., Milne, J.E., Booth, W.G., Chiocchio, F., 1993. Lake Erie offshore in 1990—restoration and resilience in the central basin. J. Great Lakes Res. 19, 291–309.

Chen, M.J., Li, X. Dai, Sun, Y., Chen, F., 2011. Effect of phosphorus and temperature on chlorophyll a contents and cell sizes of Scenedesmus obliquus and Microcystis aeruginosa. Limnology. 12, 187–192.

Chong, W., Hai-Nan, K., Xin-Ze, W., Hao-Dong, W., 2010. Effects of iron on growth and intracellular chemical contents of Microcystis aeruginosa. Biomed. Environ. Sci. 23, 48–52.

DePinto, J.V., Young, T.C., Mcllroy, L.M., 1986. Impact of phosphorus control measures on water quality of the Great Lakes. Environ. Sci. Technol. 20, 752–759.

Dolan, D.M., 1993. Point source loadings of phosphorus to Lake Erie: 1986–1990. J. Great Lakes Res. 19, 212–223.

Dunker, S., Jakob, T., Wilhelm, C., 2013. Contrasting effects of the cyanobacterium *Microcystis aeruginosa* on the growth and physiology of two green algae, *Oocystis marsonii* and *Scenedesmus obliquus*, revealed by flow cytometry. Freshw. Biol. 58, 1573–1587.

Fahnenstiel, G.L., Sayers, M.J., Shuchman, R.A., Yousef, F., Pothoven, S.A., 2016. Lake-wide phytoplankton production and abundance in the Upper Great Lakes: 2010–2013. J. Great Lakes Res. 42 (3), 619–629.

GLWQA (Great Lakes Water Quality Agreement), 1978. International Joint Commission, IJC, Great Lakes Water Quality Agreement of. Agreement with Annexes and Terms of Reference, Between the United States of America and Canada. International Joint Commission, Windsor, Ontario, p. 1978.

GLWQA (Great Lakes Water Quality Agreement). 2016. The United States and Canada Adopt Phosphorus Load Reduction Targets to Combat Lake Erie Algal Blooms. https://binational.net/2016/02/22/finalptargets-ciblesfinalesdep. Viewed 25 Feb 2016.

Heisler, J., Glibert, P.M., Burkholder, J.M., Anderson, D.M., Cochlan, W., Dennison, W.C., Dortch, Q., Gobler, C.J., Heil, C.A., Humphries, E., Lewitus, A., 2008. Eutrophication and harmful algal blooms: a scientific consensus. Harmful Algae 8 (1), 3–13.

Hondorp, D.W., Breitburg, D.L., Davias, L.A., 2010. Eutrophication and fisheries: separating the effects of nitrogen loads and hypoxia on the pelagic-to-demersal ratio and other measures of landings composition. Marine and Coastal Fisheries: Dynamics, Management, and Ecosystem Science. 2 pp. 339–361.

Hu, W. 2014. Dry Weight and Cell Density of Individual Algal and Cyanobacterial Cells for Algae Research and Development. MS Thesis, University of Missouri-Columbia 81 pg.

IJC 2017. Draft domestic action plans for achieving phosphorus reductions in Lake Erie: https://binational.net/2017/03/10/dap-pan/

Jiang, L., Xia, M., Ludsin, S.A., Rutherford, E.S., Mason, D.M., Jarrin, J.M., Pangle, K.L., 2015. Biophysical modeling assessment of the drivers for plankton dynamics in dreissenid-colonized western Lake Erie. Ecol. Model. 308, 18–33.

Kelly, J.R., Yurista, P., Starry, M., Scharold, J., Bartsch, W., Cotter, A., 2015. Exploration of spatial variability in nearshore water quality using the first Great Lakes National Coastal Condition Assessment survey. J. Great Lakes Res. 41 (4), 1060–1074.

Lambert, R.S., 2012. Great Lakes Tributary Phosphorus Bioavailability. Michigan Tech University.

Lee, G. Jones, R. Rast, W. 1980. Availability of phosphorus to phytoplankton and its implications for phosphorus management strategies, in: Loehr, R. Martin, C. Rast, W. (Eds.), Phosphorus Management Strategies for Lakes. Ann Arbor Science, Ann Arbor, MI.

Lee, S.J., Jang, M.-H., Kim, H.-S., Yoon, B.-D., Oh, H.-M., 2000. Variation of microcystin content of *Microcystis aeruginosa* relative to medium N:P ratio and growth stage. J. Appl. Microbiol. 89, 323–329.

Long, B.M., Jones, G.J., Orr, P.T., 2001. Cellular microcystin content in N-limited Microcystis aeruginosa can be predicted from growth rate. Appl. Environ. Microbiol. 67, 278–283.

Ludsin, S.A., Kershner, M.W., Blocksom, K.A., Knight, R.L., Stein, R.A., 2001. Life after death in Lake Erie: nutrient controls drive fish species richness, rehabilitation. Ecol. Appl. 11, 731–746.

Makarewicz, J.C., Bertram, P., 1991. Evidence for the restoration of the Lake Erie ecosystem. Bioscience. 41, 216–223.

Makarewicz, J.C. Lewis, T. Bertram, P. 1989. Phytoplankton and zooplankton composition, abundance and distribution and trophic interactions: offshore region of lakes Erie, Lake Huron, and Lake Michigan. 15 (1985 CIESIN).

Michalak, A.M., Anderson, E.J., Beletsky, D., Boland, S., Bosch, N.S., Bridgeman, T.B., Chaffin, J.D., Cho, K., Confesor, R., Daloğlu, I., DePinto, J.V., 2013. Record-setting algal bloom in Lake Erie caused by agricultural and meteorological trends consistent with expected future conditions. Proc. Natl. Acad. Sci. 110 (16), 6448–6452.

Obenour, D., Gronewold, A., Stow, C.A., Scavia, D., 2014. Using a Bayesian hierarchical model to improve Lake Erie cyanobacteria bloom forecasts. Water Resour. Res. 50, 7847–7860.

Ohio, E.P.A, 2010. Ohio Lake Erie Phosphorus Task Force Final Report (Ohio EPA OH Task Force).

Otten, T.G., Paerl, H.W., 2015. Health effects of toxic cyanobacteria in US drinking and recreational waters: our current understanding and proposed direction. Current environmental health reports. 2 (1), 75–84.

Pearsall, D., de Grammont, P.C., Cavalieri, C., Chu, C., Doran, P., Elbing, L., Ewert, D., Hall, K., Herbert, M., Khoury, M., Kraus, D., 2012. Returning to a healthy lake: Lake Erie biodiversity conservation strategy. Technical Report. A Joint Publication of the Nature Conservancy. Nature Conservancy of Canada, and Michigan Natural Features Inventory.

Pick, F.R., 2016. Blooming algae: a Canadian perspective on the rise of toxic cyanobacteria. Can. J. Fish. Aquat. Sci. 73 (7), 1149–1158.

R Core Team. 2016. R: A language and environment for statistical computing. R Foundation for Statistical Computing, Vienna, Austria. https://www.R-project.org/

Reichert, J.M., Fryer, B.J., Pangle, K.L., Johnson, T.B., Tyson, J.T., Drelich, A.B., Ludsin, S.A., 2010. River-plume use during the pelagic larval stage benefits recruitment of a lentic fish. Can. J. Fish. Aquat. Sci. 67 (6), 987–1004.

Rosa, F., Burns, N.M., 1987. Lake Erie central basin oxygen depletion changes from 1929–1980. J. Great Lakes Res. 13 (4), 684–696.

Rucinski, D., Scavia, D., DePinto, J., Beletsky, D., 2014. Lake Erie's hypoxia response to nutrient loads and meteorological variability. J. Great Lakes Res. https://doi.org/10.1016/j.jglr.2014.02.003.

Sayers, M., Fahnenstiel, G.L., Shuchman, R.A., Whitley, M., 2016. Cyanobacteria blooms in three eutrophic basins of the Great Lakes: a comparative analysis using satellite remote sensing. Int. J. Remote Sens. 37, 4148–4171.

Scavia, D., Allan, J.D., Arend, K.K., Bartell, S., Beletsky, D., Bosch, N.S., ... Zhou, Y., 2014. Assessing and addressing the re-eutrophication of Lake Erie: central basin hypoxia. J. Great Lakes Res. 40 (2), 226–246.

Stumpf, R.P., Wynne, T.T., Baker, D.B., Fahnenstiel, G.L., 2012. Interannual variability of cyanobacterial blooms in Lake Erie. PLoS One 7, e42444.

Stumpf, R.P., Johnson, L.T., Wynne, T.T., Baker, D.B., 2016. Forecasting annual cyanobacterial bloom biomass to inform management decisions in Lake Erie. J. Great Lakes Res. 42 (6), 1174–1183.

Vadeboncoeur, Y., McIntyre, P.B., Vander Zanden, M.J., 2011. Borders of biodiversity: life at the edge of the world's large lakes. BioScience 61 (7), 526–537.
Verhamme, E., Redder, T., Schlea, D., Grush, J., Bratton, J., DePinto, J., 2016. Development of the Western Lake Erie Ecosystem Model (WLEEM): application to connect phosphorus loads to cyanobacteria biomass. J. Great Lakes Res. 42 (6), 1193–1205.
Weakliem, D.L., 1999. A critique of the Bayesian information criterion for model selection. Sociol. Methods Res. 27 (3), 359–397.
Winter, J.G., DeSellas, A.M., Fletcher, R., Heintsch, L., Morley, A., Nakamoto, L., Utsumi, K., 2011. Algal blooms in Ontario, Canada: increases in reports since 1994. Lake and Reservoir Management. 27 (2), 107–114.
Wynne, T.T., Stumpf, R.P., 2015. Spatial and temporal patterns in the seasonal distribution of toxic cyanobacteria in Western Lake Erie from 2002–2014. Toxins. 7, 1649–1663.
Wynne, T.T., Stumpf, R.P., Tomlinson, M.C., Dyble, J., 2010. Characterizing a cyanobacterial bloom in western Lake Erie using satellite imagery and meteorological data. Limnol. Oceanogr. 55, 2025–2036.
Zhou, Y., Obenour, D.R., Scavia, D., Johengen, T.H., Michalak, A.M., 2013. Spatial and temporal trends in Lake Erie hypoxia, 1987–2007. Environ. Sci. Technol. 47, 899–905.